˙OH radicals determined photocatalytic degradation mechanisms of gaseous styrene in TiO$_2$ system under 254 nm versus 185 nm irradiation: Combined experimental and theoretical studies

Jiangyao Chen[a,b], Zhigui He[a,d], Yuemeng Ji[a], Guiying Li[a], Taicheng An[a,b,*], Wonyong Choi[c,**]

[a] State Key Laboratory of Organic Geochemistry, Guangzhou Institute of Geochemistry, Chinese Academy of Sciences, Guangzhou 510640, China
[b] Guangzhou Key Laboratory Environmental Catalysis and Pollution Control, Guangdong Key Laboratory of Environmental Catalysis and Health Risk Control, School of Environmental Science and Engineering, Institute of Environmental Health and Pollution Control, Guangdong University of Technology, Guangzhou 510006, China
[c] Division of Environmental Science and Engineering, Pohang University of Science and Technology (POSTECH), Pohang 37673, Republic of Korea
[d] University of Chinese Academy of Sciences, Beijing 100049, China

ABSTRACT

The photocatalytic transformation mechanisms of styrene, were compared in TiO$_2$ system under ultraviolet (UV) and vacuum ultraviolet (VUV) irradiations. TiO$_2$/VUV displayed higher photocatalytic degradation and mineralization efficiencies (100% and 51% within 8 min) than TiO$_2$/UV (86% and 21% within 60 min), and the increased efficiencies were contributed from enhanced production of ˙OH through VUV photolysis of H$_2$O and O$_2$. The addition reactions of these enhanced ˙OH converted styrene to benzaldehyde and other small molecular carbonyl compounds in TiO$_2$/VUV gas system. Due to absence of atmospheric ˙OH in TiO$_2$/UV system, styrene underwent cycloisomerisation to form a bicyclic byproduct, benzocyclobutene, which further transformed to benzocyclobutenone, benzocyclobutenol, phthalan, phthalide and phthalic anhydride on photocatalyst TiO$_2$. Meanwhile, both systems shared same pathways from styrene to monoaromatic alcohols, ketones, aldehydes on TiO$_2$ through ˙OH addition. Our results provide a deep insight into ˙OH-determined photocatalytic transformation mechanism of AHs and their final fate in atmospheric environment.

1. Introduction

Aromatic hydrocarbons (AHs) are a representative class of volatile organic compounds, which have been widely identified in urban and industrial regions as well as indoor environment [1–3]. Transformation of AHs in atmospheric environment leads to the formation of secondary organic aerosols (SOA) and tropospheric ozone, which significantly affect the physicochemical processes of global environment [4,5]. Long-term exposure to AHs also causes adverse effects on human health, such as headache, respiratory tract irritation, dizziness, and even carcinogenicity [6,7]. Therefore, the destructive removal of AHs has been investigated in various methods, and semiconductor photocatalysis has been extensively tested for this purpose because it operates at ambient temperature and pressure condition without the need of any chemical oxidants [8–12]. Although the final products of the photocatalytic degradation of AHs are CO$_2$ and H$_2$O, a large variety of organic intermediates and byproducts are often produced along with the

decomposition of parent AHs [13]. Some of these intermediates may pose greater threat to ecological environment and human health than the parent AHs [14]. Therefore, it is necessary to systematically study the photocatalytic degradation mechanisms of AHs to estimate the health risk of the potential byproducts of AHs degradation.

The photocatalytic transformation mechanisms of AHs have been extensively attracted attention for few decades. For instance, d'Hennezel et al. studied the photocatalytic degradation of toluene on TiO$_2$, and found its transformation to monoaromatic acids, aldehydes and alcohols [15]. Then, the aromatic ring opening reaction leads to the formation of small molecular byproducts [16]. Similar transformation pathways have also been observed for the degradation of toluene [17–20] and other AHs (e.g., benzene [21], ethylbenzene [22] and xylene [23]). All these studies consistently propose that the transformation mechanisms of AHs are closely related to reactive oxygen species (ROS, such as ˙OH, ˙O, ˙O$_2$$^-$), most importantly ˙OH [24]. However, a few studies reveal that the mechanism relies on both ˙OH and

---

$^{.}O_2^{-}$ [18] or $^{.}OH$, $^{.}O$ and $^{.}O_2^{-}$ [21]. Clearly, the role of the ROS in the photocatalytic transformation mechanism is still not fully understood. On the other hand, Yang et al. reported a cyclization reaction during the aqueous photolysis of aliphatic ketones to cyclic alcohols [25]. More recently, Clifford et al. also detected two bicyclic degradation intermediates (i.e., phthalide and phthalic anhydride) from the photolysis of gaseous o-tolualdehyde [26]. These researches display different photoinduced transformation pathways of AHs in the absence of ROS. Obviously, ROS determines the photocatalytic transformation processes during AHs degradation. Unfortunately, the complete and accurate ROS (e.g., $^{.}OH$) determined transformation mechanisms of AHs remain unclear.

In this work, the photo-induced transformation mechanism of gaseous styrene in TiO_2 system was investigated under different UV illuminants. Styrene was selected as a representative AH, since it was widely used in the synthesis and manufacture of polystyrene and other copolymers, leading to its massive emission in a variety of industrial effluents [27]. Two light sources, one with a maximum emission at 254 nm (UV) and the other with a maximum wavelength at 254 nm and a smaller ($< 5\%$) emission at 185 nm (VUV), were used to generate ROS in both systems. Previous works proposed the formation of atmospheric $^{.}OH$ from H_2O decomposition in gas phase of TiO_2/VUV system [28,29]. Then, atmospheric $^{.}OH$ was expected to formed in the TiO_2/VUV system but not in TiO_2/UV system, probably resulting in different transformation pathways of styrene in these two systems. To verify this hypothesis, the composition and concentration of ROS were further measured, while their contributions to the enhanced photocatalytic degradation and mineralization efficiencies of styrene were discussed in detail. Meanwhile, the similarity and difference of intermediates in gas as well as on catalyst of TiO_2/UV and TiO_2/VUV systems were compared through the byproduct analysis employing diffuse reflectance Fourier transform-infrared spectrometry (DRIFTS) and gas chromatography-mass spectrometer (GC–MS). Combined experimental identification of intermediates and the data from quantum chemical calculations, the photocatalytic degradation transformation mechanisms of styrene in both systems were systematically compared and testified.

2. Experimental

2.1. Photocatalytic transformation experiment

The photocatalytic degradation and mineralization of gaseous styrene were performed in a self-designed fixed bed Pyrex reactor (vol. 5 L, spherical shape) [30], which had TiO_2 catalyst on the bottom and a concentrically fixed lamp. The detailed preparation procedures and characterizations of TiO_2 catalyst were described in Fig. S1 in Supporting Information (SI). A certain amount of styrene liquid was injected in the reactor to obtain initial 400 ppmv of gaseous styrene. After adsorption equilibrium, the UV or VUV light was turned on. The optical spectra of both lights in the range of 220–600 nm were recorded by a spectrometer USB2000 (Ocean Optics) (Fig. S2). The light intensity of both lamps was about 2.3 mW cm^{-2}. The distance of TiO_2 catalyst and light was fixed at 3 cm. A water bath was used to maintain the reaction temperature inside the vessel at approximately 30 ± 2 °C. The O_2 percentage and relative humidity during the photocatalytic degradation processes were maintained at 20% and 5%, respectively. The concentrations of styrene and CO_2 within 8 min for VUV systems and 60 min for UV ones were analyzed by a gas chromatograph (GC-9800) equipped with a flame ionization detector and methane converter.

2.2. ROS and intermediate analysis methods

The ROS of $^{.}OH$ and $^{.}O_2^{-}$ were detected by electron parameter resonance (EPR, Bruker EMXPlus-10/12) system using 5, 5-dimethyl-1-pyrroline N-oxide as a trapping agent after 10 min, while O_3 was

analyzed by an ozone detector (Model 106-L Seriai#1256 L, 2B Technologies, Inc.). The UV–vis (UV–vis) absorption spectrum of styrene was recorded on a UV–vis-NIR spectrophotometer (Varian Cary 300). The gaseous samples were collected in 2.7-L stainless steel canisters (Entech Instruments Inc, SiloniteTM) and then analyzed using an Entech 7100 pre-concentrator (Entech Instruments Inc., CA, USA) coupled with GC–MS (7890A GC-5975C MS, Agilent technologies, USA). Both DRIFTS (Nicolet Is10, Thermo Scientific) and GC–MS were employed to characterize and identify the intermediates adsorbed on TiO_2 catalyst. The TiO_2 catalyst after photodegradation was extracted with methanol, and then the extracted sample was re-dissolved in 1 mL ethyl acetate and subsequently injected into the GC–MS for the direct determination of intermediates. A DB-1 column (60 m × 0.32 mm × 0.25 μm, Agilent Technologies, USA) was used with GC oven temperature program: initially 35 °C for 5 min, increased to 150 °C at a rate of 5 °C min^{-1}, and then to 250 °C at a rate of 15 °C min^{-1} and finally held for another 2 min. The carrier gas was ultrahigh pure helium at a constant flow rate of 1.2 mL min^{-1}. Mass spectrometer conditions were set as follows: temperature of the transfer line at 290 °C, ionizing energy of 70 eV, and scan range of 45–260 me^{-1}. All the intermediates in gas phase and on TiO_2 catalyst were identified both via the retention time and mass spectrum by using the NIST 14 database (National Institute of Standards and Technology).

2.3. Quantum chemical calculations

All quantum chemical calculations were performed using the Gaussian 09 package [31]. The frontier electron densities (FEDs) of the highest occupied molecular orbital (HOMO) and the lowest unoccupied molecular orbital (LUMO) of styrene were determined to predict the initial attack position by ROS. Geometric optimization of all stationary points, including the reactants, products and degradation intermediates, was performed by using density functional theory. The hybrid density functional M06-2X method was adopted with the 6–311 G(d,p) basis set, i.e., at the M06-2X/6–311 G(d,p) level [5]. The dual-level potential profile was further refined with a more flexible basis set 6-311 + G (3df,3pd), i.e., at the M06-2X/6-311 + G (3df,3pd) level. For the simplicity, the dual-level approach was denoted as X//Y, where a single-point energy calculation at level X was carried out for the geometry optimized at a lower level Y, i.e., M06-2X//M06-2X in this study.

3. Results and discussion

3.1. Photocatalytic transformation of styrene in TiO_2/UV and TiO_2/VUV systems

Fig. 1 displays the photocatalytic removal of styrene and the accompanying production of CO_2 in TiO_2/UV and TiO_2/VUV systems. A continuous decrease of styrene from 400 to 56 ppmv is observed in TiO_2/UV system within 60 min, achieving 86% degradation efficiency (Fig. 1a). Meanwhile, about 672 ppmv of CO_2 is generated, indicating that 21% of styrene is converted to CO_2 in this system (Fig. 1b). On the other hand, when VUV light is irradiated instead, 400 ppmv of styrene completely disappears within only 8 min, accompanying the production of much higher concentration of CO_2 (1632 ppmv) which corresponds to the mineralization efficiencies of 51% styrene. The photocatalytic transformation efficiency of styrene in TiO_2/VUV system is by far higher than TiO_2/UV consistent with the previous study [32–34].

The photocatalytic performance seems to be influenced by the direct photolysis behavior. The direct UV photolysis removes 222 ppmv of styrene within 60 min, whereas the VUV photolysis degrades 249 ppmv of styrene just within 8 min (Fig. 1a). In addition, the production of CO_2 in VUV photolysis system (1088 ppmv) is ca. 34 times higher than that in UV photolysis system (32 ppmv) (Fig. 1b). Further comparison reveals that the removal of styrene by UV and VUV photolysis accounts for about 65% and 63% of the overall photocatalytic degradation
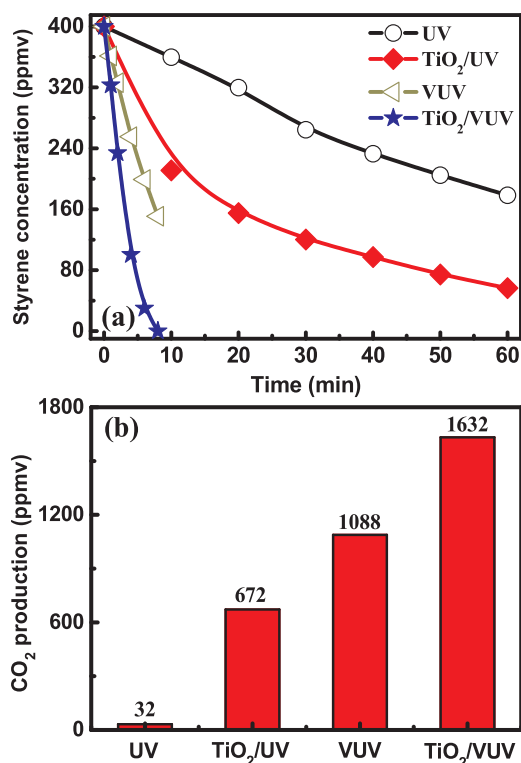
Fig. 1. Time profiles of photocatalytic degradation of styrene (a) and the accompanying production of CO_2 (b) in TiO_2/UV and TiO_2/VUV systems. (Experimental conditions: 20% (vol) O_2 and 5% relative humidity).

efficiency for two photolysis systems, respectively. This indicates that the contribution of direct photolysis to the overall removal of styrene in the photocatalytic system is the same whether UV or VUV is employed. However, the relative contribution of UV and VUV photolysis to CO_2 production is very different. As shown in Fig. 1b, VUV photolysis contributes to 67% of the overall CO_2 production in TiO_2/VUV system.

Note that this is very close to the styrene degradation efficiency (63%), suggesting that the styrene photolyzed by VUV is efficiently mineralized to CO_2. However, UV photolysis only contributes to 5% of the overall CO_2 production in TiO_2/UV system, indicating that the direct UV photolysis is very inefficient in mineralizing styrene. On the other hand, the VUV photolysis is capable of efficiently mineralizing styrene and its combination with TiO_2 makes the overall efficiencies of styrene removal and mineralization even higher. Meanwhile, the fact that direct UV photolysis is not efficient in mineralizing styrene implies that it should produce more intermediates, which should be further degraded and mineralized during the subsequent photocatalytic processes on TiO_2.

Overall, TiO_2/VUV displays much higher photocatalytic degradation and mineralization performances to styrene than TiO_2/UV, mainly ascribed to the higher photolysis activity of VUV than UV. Noted that UV and VUV display almost identical emission intensity at maximum wavelength of 254 nm (Fig. S2). Then, the effect of 254 nm wavelength in UV and VUV on TiO_2 photocatalysis should not be significant as long as the 254 nm photons are energetic enough to excite the TiO_2 band gap (3.2 eV corresponding to photons with λ < 387 nm). The excited electrons and holes (so called "hot carriers") by 185 nm in VUV should be responsible for the enhanced photocatalytic performance.

3.2. ·OH enhanced photocatalytic performance in both TiO_2/VUV and TiO_2/UV system

Photocatalytic processes generate several kinds of ROS. Identifying the roles of different ROS is essential to understand the mechanisms of photocatalytic performance in TiO_2/VUV and TiO_2/UV systems. The present photocatalytic systems have H_2O and O_2 as precursors of ROS. H_2O molecules absorb wavelengths between 175 and 190 nm [22], while O_2 molecules absorb wavelengths shorter than 243 nm [35]. Both H_2O and O_2 absorb wavelength at 185 nm to generate ·OH through the following processes (Eqs. (1)–(3)).
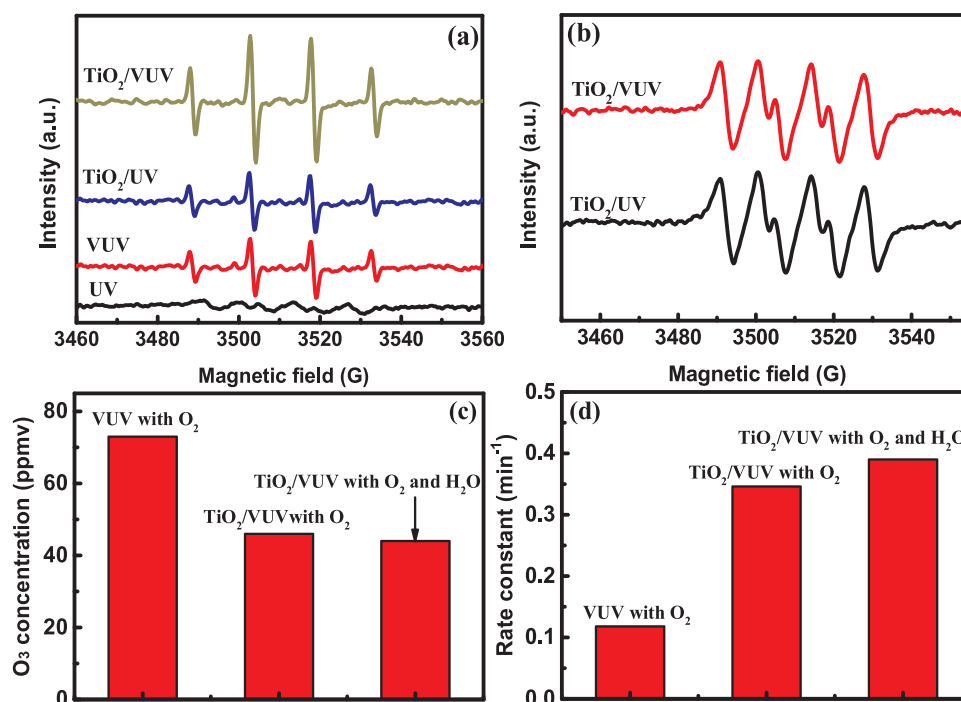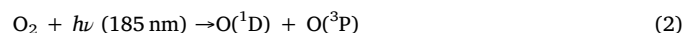
$$H_2O + h\nu\ (185\,nm) \rightarrow H + \,·OH \tag{1}$$

$$O_2 + h\nu\ (185\,nm) \rightarrow O(^1D) + O(^3P) \tag{2}$$

Fig. 2. Spin trapping EPR spectra of ·OH (a) and ·O_2^- (b), and O_3 concentration (c), rate constant (d) under different reaction conditions.
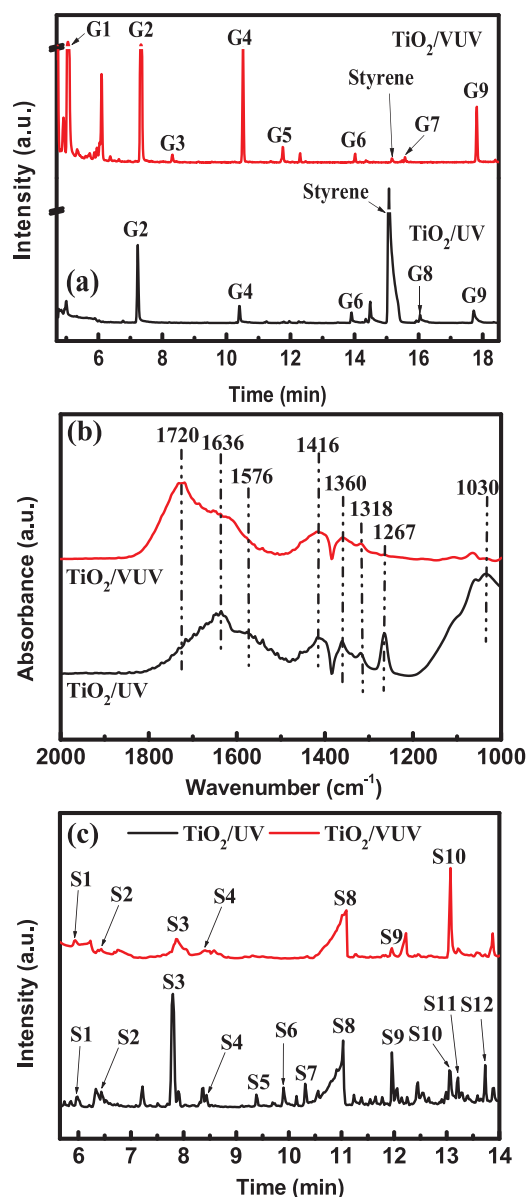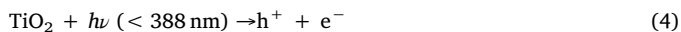
Fig. 3. Total ion chromatogram of intermediates identified in gas (a) and on catalyst (c). DRIFTS spectrum of catalyst after the photocatalytic degradation of styrene (b).

$$O(^1D) + H_2O \rightarrow 2\,^{\cdot}OH \tag{3}$$

Our EPR spin-trapping results clearly confirm strong signal of $^{\cdot}OH$ in both VUV photolysis and TiO_2/VUV systems (Fig. 2a). Also, the $^{\cdot}OH$ peak intensity in TiO_2/VUV system is observed higher than that of VUV photolysis, which indicates that $^{\cdot}OH$ radicals are additionally generated in the photocatalytic process (Eqs. (4) and (9)). Not only the transfer of H_2O by hole (Eqs. (4) and (5)), but also in-situ photocatalytic generated O_3 from O_2 can contribute to the production of $^{\cdot}OH$ (Eqs. (6) and (9)).

$$TiO_2 + h\nu\ (< 388\,nm) \rightarrow h^+ + e^- \tag{4}$$

$$H_2O + h^+ \rightarrow {}^{\cdot}OH + H^+ \tag{5}$$

$$O(^3P) + O_2 \rightarrow O_3 \tag{6}$$

$$O_3 + e^- \rightarrow {}^{\cdot}O_3{}^- \tag{7}$$

$${}^{\cdot}O_3{}^- + H^+ \rightarrow HO_3{}^{\cdot} \tag{8}$$

$$HO_3{}^{\cdot} \rightarrow O_2 + {}^{\cdot}OH \tag{9}$$

The variations of O_3 concentration under three experimental conditions: VUV with O_2, TiO_2/VUV with O_2 and TiO_2/VUV with O_2 and H_2O are then compared to investigate the contribution of O_3 to the production of $^{\cdot}OH$. As shown in Fig. 2c, about 73 ppmv of O_3 is generated under VUV irradiation in the presence of O_2 alone (Eq. (6)), while the addition of TiO_2 decreases the O_3 concentration to 46 ppmv, which indicates that about 37% of O_3 is decomposed on TiO_2 (possibly via $^{\cdot}O_3{}^-$ formation according to Eq. (7)). Further addition of H_2O leads to the decrease of the O_3 concentration to 44 ppmv, implying that H_2O efficiently accelerates the conversion of $^{\cdot}O_3{}^-$ to $^{\cdot}OH$ on TiO_2 (Eqs. (8) and (9)). Similar phenomenon is also observed by Cheng et al [22]. Clearly, a total of ca. 40% of O_3 is transformed into $^{\cdot}OH$ in TiO_2/VUV system, and the rest O_3 may directly participate in the ozonation degradation of styrene. However, the in-situ generated O_3 does not seem to serve as a main oxidant of styrene in TiO_2/VUV system. Fig. 2d also compares the styrene degradation rate constants with the in-situ generation of O_3, and clearly shows that higher concentration of O_3 does not induce faster photodegradation of styrene. Note that the photocatalytic degradation is clearly enhanced in the presence of added H_2O, which implies that additional $^{\cdot}OH$ was produced from the photolysis of H_2O. Thus, the higher degradation activity of TiO_2/VUV system is ascribed to the role of $^{\cdot}OH$ as a main oxidant.
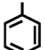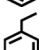
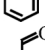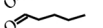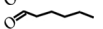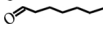$$O_2 + e^- \rightarrow {}^{\cdot}O_2{}^- \tag{10}$$

On the other hand, the reduction of O_2 by e^- on TiO_2 forms $^{\cdot}O_2{}^-$ radicals (Eq. (10)). The obvious signals of $^{\cdot}O_2{}^-$ in both TiO_2/UV and TiO_2/VUV systems solidly confirm the process of Eq. (10) (Fig. 2b). Further comparison reveals the identical intensity of $^{\cdot}O_2{}^-$ in both systems. Besides, UV and VUV possess almost identical emission intensity in the range of 220–600 nm (Fig. S2). In addition, the transformation of O_3 to $^{\cdot}O_2{}^-$ radicals on TiO_2 is also negligible, which is solidly proved by our recent published work [36]. This confirms that irradiation of 185 nm for VUV system has no direct influence on the formation of $^{\cdot}O_2{}^-$ on TiO_2. Since $^{\cdot}O_2{}^-$ is generated through the photocatalytic process which little depends on the extra photon energy exceeding the bandgap, there is little difference in its generation between UV and VUV systems. All these results reveal that the higher photocatalytic activity of TiO_2/VUV system are related with the enhanced production of $^{\cdot}OH$ through VUV photolysis of H_2O and O_2. Increasing relative humidity and O_2 percentage also does not enhance the photocatalytic rate constant toward styrene in TiO_2/UV system, but do significantly influence the rate constant in TiO_2/VUV system (Fig. S3), solidly confirming the above results.

3.3. Similarity and difference of degradation intermediates in TiO_2/UV and TiO_2/VUV systems

Results from Fig. 1b revealed that only 21%–51% of styrene was mineralized into CO_2, leaving significant intermediates in TiO_2/UV and TiO_2/VUV systems. Meanwhile, these two systems display different ROS compositions in gas phase, leading to the formation of different intermediates. As shown in total ion chromatogram of gaseous sample collected in TiO_2/UV system, a total of six peaks are observed, corresponding to six compounds (Fig. 3a). After comparing their mass fragments with GC–MS library, the one with the highest intensity is identified as styrene and the others are identified as its degradation byproducts, for example benzene (G2), toluene (G4), ethylbenzene (G6), benzocyclobutene (G8) and benzaldehyde (G9) (Table 1). Benzene, toluene and ethylbenzene are probably generated from the photodecomposition of styrene, since styrene absorbs light with wavelengths shorter than 300 nm (Fig. S4). The fragmentation of styrene to form benzene is also observed in previous work [37], consistent with our hypothesis. Differently, benzaldehyde is an oxidation byproduct, which cannot be formed in gas phase of TiO_2/UV system, due to lack of ROS. Thus, it is more likely from catalyst desorption. Different in those

Table 1

Main identified gaseous intermediates in TiO_2/UV and TiO_2/VUV systems during the degradation of styrene.

No.	Name	CAS No.	Formula	Retention time (min)	Main fragments (m/z)
In TiO_2/UV and TiO_2/VUV systems					
G2	Benzene	71-43-2		7.23	78, 63, 52, 44, 37
G4	Toluene	108-88-3		10.53	91, 74, 65, 51, 39
G6	Ethylbenzene	100-41-4		14.02	106, 91, 78, 65, 51, 44, 37
G9	Benzaldehyde	100-52-7		17.81	105, 77, 51, 44, 37
In TiO_2/UV system					
G8	Benzocyclobutene	694-87-1		16.04	104, 78, 63, 51, 39
In TiO_2/VUV system					
G1	Acetone	67-64-1		5.04	58, 43, 36
G3	Pentanal	110-62-3		8.32	86, 78, 71, 57, 44, 37
G5	Hexanal	66-25-1		11.75	82, 72, 56, 44, 37
G7	Heptanal	111-71-7		15.57	96, 81, 70, 55, 44, 37

monocyclic products, benzocyclobutene shows bicyclic structure and same molecular formula as styrene, suggesting that cycloisomerisation reaction occurs in gas phase of TiO_2/UV system.

Similar with TiO_2/UV system, styrene, benzene (G2), toluene (G4), ethylbenzene (G6) and benzaldehyde (G9) are also detected in gas phase of TiO_2/VUV system. Besides catalyst desorption, benzaldehyde also comes from reaction of styrene with gaseous $\cdot OH$ in TiO_2/VUV system before completely mineralized into CO_2, resulting lower relative content of benzaldehyde in TiO_2/VUV gas system than TiO_2/UV one. Actually, the relative contents of styrene, benzene, toluene and ethylbenzene are also far lower than that in TiO_2/UV system (the Y-axis scale of total ion chromatogram of TiO_2/VUV system is only one sixth of that for TiO_2/UV one), consistent with the higher mineralization performance of TiO_2/VUV system. Then, higher concentrated monocyclic AHs (e.g., benzene) are emitted from TiO_2/UV system, posing higher threat to the workers and surrounding residents after long-term exposure. Further observation reveals another four peaks in gas phase of TiO_2/VUV system (Fig. 3a). After comparing their mass fragments with GC–MS library, acetone (G1), pentanal (G3), hexanal (G5) and heptanal (G7) are also identified (Table 1). The detection of these small molecular carbonyl compounds indicates the reaction of benzene ring with $\cdot OH$ in gas phase of TiO_2/VUV system. Similar carbonyl compounds such as formaldehyde [38] and acetaldehyde [28] have also been found as gaseous intermediates for TiO_2/VUV photocatalysis of other AHs, consistent with our results. In addition, oxygenated compounds are believed to dominate precursors for the formation of SOA [39,40]. Then, the emitted carbonyl compounds from TiO_2/VUV system should contribute more significantly to SOA formation in real atmospheric environment. Hence, more efforts should be made to deeply reveal the contribution mechanism of these gaseous intermediates to SOA formation as well as human health threat during AH photodegradation.
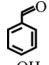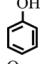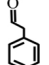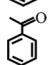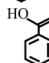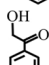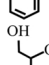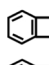
Besides gaseous byproducts, the intermediates adsorbed onto catalyst are also identified. DRIFTS are firstly used to distinguish the possible intermediates. As shown in Fig. 3b, same peaks assigned to COO-group (1318, 1360, 1416 cm^{-1}), aromatic ring (1576 and 1636 cm^{-1}) and C=O group (1720 cm^{-1}) appear in both TiO_2/UV and TiO_2/VUV systems. After carefully comparing with previous works [14,41], the appearance of same groups in this study reveals the identical formation of aromatic aldehydes, ketones and acids both in TiO_2/UV and TiO_2/VUV systems. However, two extra peaks at 1030 and 1267 $cm^{-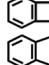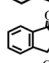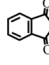1}$ are observed in TiO_2/UV system. Based on early published literatures [26,42], the former peak is characteristics of the O−H bending

vibration of cyclic alcohol, while the latter one is due to the asymmetric stretching mode of C−O−C for cyclic anhydride. These results suggest the formation of aromatic cyclic alcohol and cyclic anhydride in TiO_2/UV system.

Further qualitative analysis of above intermediates is further conducted using GC–MS. As shown in Fig. 3c, a total of seven peaks are identified in total ion chromatogram of TiO_2/VUV system, corresponding to seven byproducts. After comparing their fragments with mass library, these byproducts are confirmed as benzaldehyde (S1), phenol (S2), phenylacetaldehyde (S3), acetophenone (S4), benzoic acid (S8), 2-hydroxy-1-phenylethanone (S9) and 1-phenyl-1,2-ethanediol (S10), respectively (Table 2). These seven byproducts are also detected in TiO_2/UV system. And same composition of ROS ($\cdot OH$ and $\cdot O_2^-$) on catalyst of TiO_2/UV and TiO_2/VUV systems are responsible for these same byproducts. Previous researches reported the formation of similar intermediates (e.g., acetophenone [43], benzaldehyde [44], benzoic acid [45], phenol [22]) on TiO_2 during the degradation of other AHs (e.g., toluene and ethylbenzene) in $\cdot OH$ involved systems. Then, styrene probably also undergoes $\cdot OH$-induced transformation pathways in our study. Furthermore, another five peaks are also detected in the total ion chromatogram of TiO_2/UV system, and they are identified as benzocyclobutenone (S5), benzocyclobutenol (S6), phthalan (S7), phthalide (S11) and phthalic anhydride (S12) after comparing their mass fragments with GC–MS library (Table 2). These five compounds are all contained oxygenated bicyclic structures, which are similar to benzocyclobutene, implying that benzocyclobutene reacts with $\cdot OH$ on TiO_2 to form those oxygenated bicyclic compounds. Moreover, these oxygenated bicyclic compounds show low volatilities, probably contributing more significantly to SOA formation and growth of small particles in real atmospheric environment. For example, in the work of Clifford et al., phthalide and phthalic anhydride was detected in particle phase [26], solidly proving our hypothesis of the important atmospheric environmental implication of these bicyclic compounds.

In summary, the similar conclusion obtained that TiO_2/UV and TiO_2/VUV systems generate some common intermediates in gas (e.g., benzene, toluene, ethylbenzene) and on catalyst (e.g., 1-phenyl-1,2-ethanediol, acetophenone, phenylacetaldehyde). Differently, benzocyclobutenone and its derivative products are obtained in TiO_2/UV system, while benzaldehyde and small molecular carbonyl compounds are obtained in gaseous phase of TiO_2/VUV system. All these similar and different intermediate results imply that styrene undergoes same surfaced reaction onto TiO_2 and also different atmospheric

Table 2
Main identified adsorbed intermediates on the catalyst in TiO$_2$/UV and TiO$_2$/VUV systems during the degradation of styrene.

NO.	Name	CAS No.	Formula	Retention time (min)	Main fragments (m/z)
In TiO$_2$/UV and TiO$_2$/VUV systems					
S1	Benzaldehyde	100-52-7		5.98	106, 77, 51
S2	Phenol	108-95-2		6.47	94, 66, 39
S3	Phenylacetaldehyde	122-78-1		7.79	120, 91, 65, 39
S4	Acetophenone	98-86-2		8.45	120, 105, 77, 51, 32
S8	Benzoic acid	65-85-0		11.04	122, 105, 77, 51, 37
S9	2-Hydroxy-1-phenylethanone	582-24-1		11.96	136, 105, 77, 51
S10	1-Phenyl-1,2-ethanediol	93-56-1		13.06	138, 107, 79, 51, 31
In TiO$_2$/UV system					
S5	Benzocyclobutenone	3469-06-5		9.39	118, 89, 63, 39
S6	Benzocyclobutenol	35447-99-5		9.90	119, 91, 65, 39
S7	Phthalan	496-14-0		10.31	120, 91, 65, 39
S11	Phthalide	87-41-2		13.22	134, 105, 77, 51
S12	Phthalic anhydride	85-44-9		13.73	148, 104, 76, 50

transformation pathways of ˙OH radicals in TiO$_2$/UV and TiO$_2$/VUV systems.

3.4. Revelation of styrene transformation mechanisms in TiO$_2$/UV and TiO$_2$/VUV systems by combined experimental and theoretical methods

To accurately elucidate the photocatalytic transformation mechanism of styrene both in TiO$_2$/UV and TiO$_2$/VUV systems, quantum chemical calculations were also performed cooperated with the intermediate results. Firstly, the FED and point charge calculations of styrene molecule reveal the initial reaction site of terminal carbon atom for styrene's vinyl group (C8), due to its much higher FED values at the highest (0.2415) and lowest (0.3558) unoccupied molecular orbitals (Table S1). Meanwhile, the most negative point charge of the atom (-0.345) further confirms the above deduction. Our previous theoretical calculation also revealed that ˙OH addition more easily happened on the side chain of styrene than H abstraction [46].

Then in gas phase of TiO$_2$/VUV system, ˙OH firstly adds onto C8 of styrene to form 2-phenylethyl alcohol radical. Theoretical calculation reveals significant energy was released during this reaction ($\triangle E_r$ = -36.11 kcal mol^{-1}), suggesting a thermodynamically favorable process (Fig. 4a). Since existence of abundant O$_2$ in the reactor, this radical is then oxidized by O$_2$ to form O$_2$-2-phenylethyl alcohol adduct with a high exothermic energy ($\triangle E_r$ = -15.08 kcal mol^{-1}), verifying a spontaneous reaction of the formation of this adduct. Furthermore, the intramolecular hydrogen shift from hydroxyl group to peroxy radical site via six-membered ring transition state happens on this adduct to form a weakly bound radical, which then dissociates to form benzaldehyde. The theoretical calculation also reveals a significant release of energy ($\triangle E_r$ = -38.28 kcal mol^{-1}) for above reactions, confirming easily happening of the transformation of O$_2$-2-phenylethyl alcohol adduct to benzaldehyde. Our results are in line with that proposed by Bignozzi
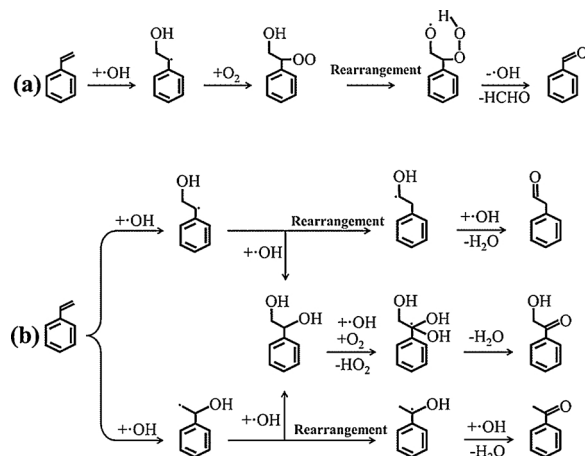

Fig. 4. Transformation mechanisms of styrene in TiO$_2$/VUV gas system (a) and on catalyst of TiO$_2$/UV and TiO$_2$/VUV systems (b).

et al. who found that the maximum yield of gaseous benzaldehyde from styrene oxidation by ˙OH was approximately 60% [47]. Under further attack of ˙OH, benzaldehyde undergoes ring-opening process to form a series of ring-opening carbonyl compounds (e.g., heptanal, hexanal, pentanal and acetone). The above ring-opening pathways are consisted with the results reported by Zhao et al. [37].

In the meantime, the addition reaction of ˙OH onto C8 of styrene also occurs on TiO$_2$ of TiO$_2$/VUV system, leads to the formation of two radicals, 2-phenylethyl alcohol radical and 1-phenylethyl alcohol radical (Fig. 4b), releasing comparatively high energies ($\triangle E_r$ = -36.11 and -27.70 kcal mol^{-1}). Then, both radicals react with ˙OH to form same aromatic diol (1-phenyl-1,2-ethanediol). The much large disparity

of reaction energies ($\triangle E_r$ = -86.40 and 3.36 kcal mol^{-1}) for those two ·OH addition reactions reveals more favorable transformation of 2-phenylethyl alcohol radical to the diol. Finally, this diol is transformed to 2-hydroxy-1-phenylethanone under the both reactions of ·OH and O$_2$, releasing much high energy ($\triangle E_r$ = -82.21 kcal mol^{-1}). Besides transformation to above diol, the rearrangement reactions occur on 2-phenylethyl alcohol radical and 1-phenylethyl alcohol radical. The theoretical reaction energies for above two reactions are obtained as 3.70 and -19.50 kcal mol^{-1}, respectively. The much lower energy released from 2-phenylethyl alcohol radical rearrangement reaction than ·OH addition one reveals the preferential happening of the latter reaction. However, 1-phenylethyl alcohol radical shows the opposite result. Anyway, under further attack by ·OH, the rearranged radicals are finally converted into phenylacetaldehyde and acetophenone, releasing significantly high energies ($\triangle E_r$ = -89.91 and -83.60 kcal mol^{-1} respectively).

Completely same transformation pathways of styrene to 2-hydroxy-1-phenylethanone are observed that phenylacetaldehyde and acetophenone are obtained on catalyst of TiO$_2$/UV system. However, some different atmospheric transformation processes are also observed in this system. Since the absent of atmospheric ·OH, the transformation of styrene to benzaldehyde is unable to occur in gas phase of TiO$_2$/UV system. Instead, a cycloisomerisation reaction for styrene happens to form benzocyclobutene (Fig. 5a). The happening of this reaction may be due to that the energy of the UV photon (471 kJ mol^{-1}) is weaker than C=C bond (615 kJ mol^{-1}) [48], but can break π bond (264 kJ mol^{-1}) of C=C bond. The correspondingly theoretical calculated reaction energy needed for above cycloisomerisation process is approximately 11.90 kcal mol^{-1}, which is by far lower than UV photon energy, revealing it is not a difficult reaction under UV irradiation. This result is also completely confirmed by the conclusion of Yu et al. [49] that extensive hydrogen interchange occurred between aromatic ring and side chain in the excited state to mainly suppress the dissociation rate, facilitating the cycloisomerisation of styrene to benzocyclobutene.

Then, after benzocyclobutene approaching to TiO$_2$, it easily reacts with interfacial ·OH to initially form 2−OH-benzocyclobutene radical, benzocyclobutene radical and then benzocyclobutenol. The above reactions release of a total energy of 113.13 kcal mol^{-1}, indicating thermodynamically favorable transformation of benzocyclobutene to benzocyclobutenol induced by ·OH. Furthermore, this alcohol is oxidized by O$_2$ to generate 2−OH-benzocyclobutenol radical, which then reacts

with ·OH to form 2,2-diOH-benzocyclobutenol and finally benzocyclobutenone. Our theoretical calculation reaction energy of -87.27 kcal mol^{-1} reveals the spontaneous transformation from alcohol to ketone on TiO$_2$ with the reaction with both O$_2$ and ·OH. On the other hand, ·OH addition on benzocyclobutene splits its four-membered ring to form 1,2-benzenedimethanol radical, which subsequently converts into phthalan after losing one H$_2$O (Fig. 5b). Approximately 35.55 kcal mol^{-1} of energy is released during this process, suggesting that the transformation of benzocyclobutene to phthalan is spontaneous. However, this released energy is about 31% of that for the transformation from benzocyclobutene to benzocyclobutenol (Fig. 5a), suggesting that the secondary transformation route of benzocyclobutene to phthalan. Further ·OH addition to phthalan leads to the formation of phthalan radical, 2−OH-phthalan radical and then 2,2-diOH-phthalan. Finally, phthalide was formed after 2,2-diOH-phthalan loses one H$_2$O. The released energy during the transformation of phthalan to phthalide is calculated as -112.71 kcal mol^{-1}, solidly proving the easily occurring of those processes. Finally, under the effect of ·OH, phthalide undergoes similar pathways to generate phthalic anhydride, releasing higher energy of -208.95 kcal mol^{-1}. And after comparing with the released energies of all transformation pathways in TiO$_2$/UV system, it is found that styrene prefers to transform to oxygenated bicyclic compounds ($\triangle E_r$ > -188 kcal mol^{-1}) rather than to oxygenated monocyclic ones ($\triangle E_r$ > -107 kcal mol^{-1}).

Furthermore, above photocatalytic degradation mechanism results clearly concluded the determined role of ·OH during styrene photocatalysis treatment. That is to say, by regulating ·OH distribution in styrene photocatalysis system, carbonyl or bicyclic compounds is selectively produced. And in our recent published work [36], both ·OH and ·O$_2^-$ were proved important for the epoxidation transformation of n-hexane, while ·OH dominated in the conversion of alcohol intermediates to corresponding radicals, and ·O$_2^-$ determined the subsequent epoxidation transformations of these radicals to epoxides. Based on these results, the correlation of ROS and byproduct is easily established, to avoid the generation of intermediates to pose higher threat to environment and human health than the parent organics, according to precise regulation reaction mechanism of ROS produced in both systems, facilitating the promotion of performance and environmental friendliness of photocatalysis technology. Also, our mechanism results are applicable for the fate evaluation of styrene in real atmospheric environment: conversion of styrene to carbonyl compounds with enough ·OH (e.g., daytime), while to oxygenated bicyclic compounds when ·OH is not enough (e.g., nighttime). This finding is helpful to understand the similarities and differences of AH photocatalytic transformation process and contribution to SOA formation in the atmospheric environment at day and night time. And more studies are necessary to accurately assess the impacts of AHs on SOA formation with the involvement of ROS, which requires the integrated consideration of ROS generation, composition and concentration as well as AH emission, migration and transformation.

4. Conclusions

The combined experimental and theoretical investigations on transformation mechanism of gaseous styrene in TiO$_2$/UV and TiO$_2$/VUV systems were conducted. Much higher degradation and mineralization transformations were obtained in TiO$_2$/VUV than TiO$_2$/UV system, due to the increased ·OH. Moreover, ·OH ensured the conversion of styrene to carbonyl compounds in gas phase, and to alcohols, ketones and aldehydes on TiO$_2$ before mineralized to CO$_2$. When absent of atmospheric ·OH in gas phase, styrene initially cycloisomerised to benzocyclobutene, and then spontaneously converted into more refractory compounds. Therefore, the findings in this study were highly helpful to comprehensively understand the transformation mechanism and accurately evaluate the fate of AHs during the photolytic and photocatalytic treatment process.
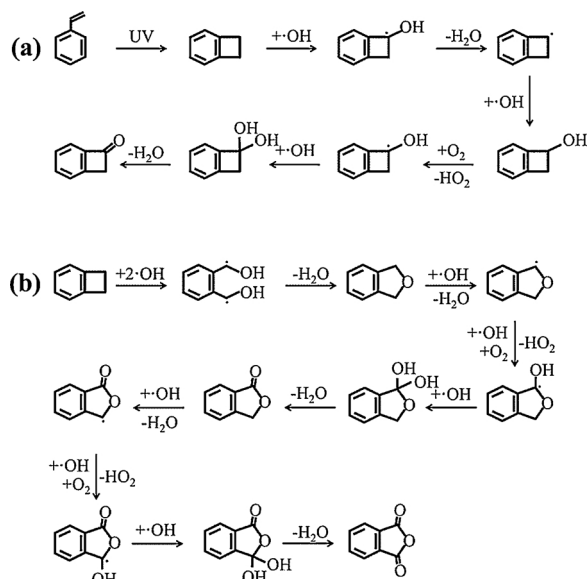

Fig. 5. Transformation mechanisms of styrene in gas (a) and on catalyst (a, b) of TiO$_2$/UV system.

Declarations of interest

None.

Acknowledgements

Appendix A. Supplementary data

Supplementary material related to this article can be found, in the online version, at doi:https://doi.org/10.1016/j.apcatb.2019.117912.

References

[1] E. Ilgen, K. Levsen, J. Angerer, P. Schneider, J. Heinrich, H.E. Wichmann, Atmos. Environ. 35 (2001) 1253–1264.

[2] J.P. Zhu, S.L. Wong, S. Cakmak, Environ. Sci. Technol. 47 (2013) 13276–13283.

[3] M. Hahm, J. Lee, M.Y. Lee, S.H. Byeon, Hum. Ecol. Risk Assess. 22 (2016) 1312–1322.

[4] B.J. Finlayson-Pitts, J.N. Pitts, Science 276 (1997) 1045–1051.

[5] Y.M. Ji, J. Zhao, H. Terazono, K. Misawa, N.P. Levitt, Y.X. Li, Y. Lin, J.F. Peng, Y. Wang, L. Duan, B.W. Pan, F. Zhang, X.D. Feng, T.C. An, W. Marrero-Ortiz, J. Secrest, A.L. Zhang, K. Shibuya, M.J. Molina, R.Y. Zhang, Proc. Natl. Acad. Sci. U. S. A. 114 (2017) 8169–8174.

[6] J.T. Cohen, G. Carlson, G. Charnley, D. Coggon, E. Delzell, J.D. Graham, H. Greim, D. Krewski, M. Medinsky, J. Toxicol. Environ. Health B 5 (2002) 1–263.

[7] P. Dalton, B. Cowart, D. Dilks, M. Gould, P.S.J. Lees, A. Stefaniak, E. Emmett, Am. J. Ind. Med. 44 (2003) 1–11.

[8] D.S. Muggli, L.F. Ding, Appl. Catal. B Environ. 32 (2001) 181–194.

[9] G.Q. Lu, M. Lim, Y. Zhou, B. Wood, L.Z. Wang, V. Rudolph, Environ. Sci. Technol. 43 (2009) 538–543.

[10] T.C. An, L. Sun, G.Y. Li, Y.P. Gao, G.G. Ying, Appl. Catal. B Environ. 102 (2011) 140–146.

[11] T.C. An, J.Y. Chen, X. Nie, G.Y. Li, H.M. Zhang, X.L. Liu, H.J. Zhao, ACS Appl. Mater. Interfaces 4 (2012) 5988–5996.

[12] J.Y. Chen, Z.G. He, G.Y. Li, T.C. An, H.X. Shi, Y.Z. Li, Appl. Catal. B Environ. 209 (2017) 146–154.

[13] A.H. Mamaghani, F. Haghighat, C.S. Lee, Appl. Catal. B Environ. 203 (2017) 247–269.

[14] T.C. An, L. Sun, G.Y. Li, S.G. Wan, J. Mol. Catal. A Chem. 333 (2010) 128–135.

[15] O. d'Hennezel, P. Pichat, D.F. Ollis, J. Photochem. Photobiol. A 118 (1998) 197–204.

[16] J.H. Mo, Y.P. Zhang, Q.J. Xu, Y.F. Zhu, J.J. Lamson, R.Y. Zhao, Appl. Catal. B Environ. 89 (2009) 570–576.

[17] S.H. Zhan, Y. Yang, X.C. Gao, H.B. Yu, S.S. Yang, D.D. Zhu, Y. Li, Catal. Today 225 (2014) 10–17.

[18] M. Sleiman, P. Conchon, C. Ferronato, J.M. Chovelon, Appl. Catal. B Environ. 86 (2009) 159–165.

[19] S. Ardizzone, C.L. Bianchi, G. Cappelletti, A. Naldoni, C. Pirola, Environ. Sci. Technol. 42 (2008) 6671–6676.

[20] T. Guo, Z.P. Bai, C. Wu, T. Zhu, Appl. Catal. B Environ. 79 (2008) 171–178.

[21] H.L. Huang, H.B. Huang, Y.J. Zhan, G.Y. Liu, X.M. Wang, H.X. Lu, L. Xiao, Q.Y. Feng, D.Y.C. Leung, Appl. Catal. B Environ. 186 (2016) 62–68.

[22] Z.W. Cheng, P.F. Sun, Y.F. Jiang, J.M. Yu, J.M. Chen, Chem. Eng. J. 228 (2013) 1003–1010.

[23] I. Dhada, M. Sharma, P.K. Nagar, J. Hazard. Mater. 316 (2016) 1–10.

[24] L.X. Zhong, F. Haghighat, C.S. Lee, Build. Environ. 62 (2013) 155–166.

[25] N.C. Yang, D.D.H. Yang, J. Am. Chem. Soc. 80 (1958) 2913–2914.

[26] G.M. Clifford, A. Hadj-Aissa, R.M. Healy, A. Mellouki, A. Munoz, K. Wirtz, M.M. Reviejo, E. Borras, J.C. Wenger, Environ. Sci. Technol. 45 (2011) 9649–9657.

[27] G. MJ, Styrene Copolymers, Marcel Dekker, New York, 1997.

[28] J. Jeong, K. Sekiguchi, W. Lee, K. Sakamoto, J. Photochem. Photobiol. A 169 (2005) 279–287.

[29] P.Y. Zhang, J. Liu, Z.L. Zhang, Chem. Lett. 33 (2004) 1242–1243.

[30] L. Sun, G.Y. Li, S.G. Wan, T.C. An, Chemosphere 78 (2010) 313–318.

[31] M.J. Frisch, G.W. Trucks, H.B. Schlegel, G.E. Scuseria, M.A. Robb, J.R. Cheeseman, G. Scalmani, V. Barone, B. Mennucci, G.A. Petersson, H. Nakatsuji, M. Caricato, X. Li, H.P. Hratchian, A.F. Izmaylov, J. Bloino, G. Zheng, J.L. Sonnenberg, M. Hada, M. Ehara, K. Toyota, R. Fukuda, J. Hasegawa, M. Ishida, T. Nakajima, Y. Honda, O. Kitao, H. Nakai, T. Vreven, J.A. Montgomery Jr., J.E. Peralta, F. Ogliaro, M.J. Bearpark, J. Heyd, E.N. Brothers, K.N. Kudin, V.N. Staroverov, R. Kobayashi, J. Normand, K. Raghavachari, A.P. Rendell, J.C. Burant, S.S. Iyengar, J. Tomasi, M. Cossi, N. Rega, N.J. Millam, M. Klene, J.E. Knox, J.B. Cross, V. Bakken, C. Adamo, J. Jaramillo, R. Gomperts, R.E. Stratmann, O. Yazyev, A.J. Austin, R. Cammi, C. Pomelli, J.W. Ochterski, R.L. Martin, K. Morokuma, V.G. Zakrzewski, G.A. Voth, P. Salvador, J.J. Dannenberg, S. Dapprich, A.D. Daniels, Ö. Farkas, J.B. Foresman, J.V. Ortiz, J. Cioslowski, D.J. Fox, Gaussian 09, Gaussian, Inc., Wallingford, CT, USA, (2009).

[32] D. Farhanian, F. Haghighat, Build. Environ. 72 (2014) 34–43.

[33] L.X. Zhong, F. Haghighat, C.S. Lee, N. Lakdawala, J. Hazard. Mater. 261 (2013) 130–138.

[34] L.P. Yang, Z.Y. Liu, J.W. Shi, Y.Q. Zhang, H. Hu, W.F. Shangguan, Sep. Purif. Technol. 54 (2007) 204–211.

[35] J. Kim, P.Y. Zhang, J.G. Li, J.L. Wang, P.F. Fu, Chem. Eng. J. 252 (2014) 337–345.

[36] P. Wei, D.D. Qin, J.Y. Chen, Y.X. Li, M.C. Wen, Y.M. Ji, G.Y. Li, T.C. An, Environ. Sci. Nano 6 (2019) 959–969.

[37] W.R. Zhao, Y.A. Yang, J.S. Dai, F.F. Liu, Y. Wang, Chemosphere 91 (2013) 1002–1008.

[38] N. Quici, M.L. Vera, H. Choi, G.L. Puma, D.D. Dionysiou, M.I. Litter, H. Destaillats, Appl. Catal. B Environ. 95 (2010) 312–319.

[39] Y. Chen, S.R. Tong, J. Wang, C. Peng, M.F. Ge, X.F. Xie, J. Sun, Environ. Sci. Technol. 52 (2018) 11612–11620.

[40] Y.M. Ji, J. Zheng, D.D. Qin, Y.X. Li, Y.P. Gao, M.J. Yao, X.Y. Chen, G.Y. Li, T.C. An, R.Y. Zhang, Environ. Sci. Technol. 52 (2018) 11169–11177.

[41] A.J. Maira, J.M. Coronado, V. Augugliaro, K.L. Yeung, J.C. Conesa, J. Soria, J. Catal. 202 (2001) 413–420.

[42] S.Y. Lin, W.T. Cheng, Y.S. Wei, H.L. Lin, Polym. J. 43 (2011) 577–580.

[43] Z.W. Cheng, L. Feng, J.M. Chen, J.M. Yu, Y.F. Jiang, J. Hazard. Mater. 254 (2013) 354–363.

[44] M.C. Blount, J.L. Falconer, J. Catal. 200 (2001) 21–33.

[45] L.X. Cao, Z. Gao, S.L. Suib, T.N. Obee, S.O. Hay, J.D. Freihaut, J. Catal. 196 (2000) 253–261.

[46] H.H. Wang, Y.M. Ji, J.Y. Chen, G.Y. Li, T.C. An, Sci. Rep. 5 (2015), https://doi.org/10.1038/srep15059.

[47] C.A. Bignozzi, A. Maldotti, C. Chiorboli, C. Bartocci, V. Carassiti, Int. J. Chem. Kinet. 13 (1981) 1235–1242.

[48] P. Kiattisaksiri, E. Khan, P. Punyapalakul, T. Ratpukdi, Water Res. 98 (2016) 160–167.

[49] C. Yu, F. Youngs, R. Bersohn, N. Turro, J. Phys. Chem. 89 (1985) 4409–4412.